Electronic Supplementary Information (ESI) for *Dalton Transactions*

pH-Controlled Assembly of Two Novel Dawson-Sandwiched Clusters Involving *In Situ* Reorganization of Trivacant α-$[P_2W_{15}O_{56}]^{12-}$ into Divacant α-$[P_2W_{16}O_{57}]^{8-}$

Ling-Yu Guo,[a,‡] Marko Jagodič,[b,‡] Su-Yuan Zeng,[c] Zvonko Jagličić,[b] Zhi-Qiang Shi,[a] Zhi Wang,[a] Xing-Po Wang,[a] Chen-Ho Tung,[a] Di Sun*,[a]

[a]*Key Lab of Colloid and Interface Chemistry, Ministry of Education, School of Chemistry and Chemical Engineering, Shandong University, Jinan, 250100, P. R. China. Email: dsun@sdu.edu.cn*

[b]*Faculty of Civil and Geodetic Engineering & Institute of Mathematics, Physics and Mechanics, University of Ljubljana, Jamova 2, 1000 Ljubljana, Slovenia.*

[c]*School of Chemistry and Chemical Engineering, Liaocheng University, Liaocheng, People's Republic of China.*

[‡] *These authors contributed equally.*

1. X-ray Single-Crystal Crystallography.

The intensity data of **1** and **2** were collected on a Bruker APEX II CCD diffractometer at 298(2) K with a graphite-monochromated Mo Kα radiation source (λ = 0.7107 Å), using ω scans to generate 3 sets for 1 and 2 of frames at different ϕ angles with a frame width of 0.5°. The collected frames were integrated with the Bruker SAINT package with a narrow frame algorithm.[1] An empirical absorption correction based on symmetry equivalent reflections was applied using the SADABS program.[2] The structures were solved by direct methods, and all non-hydrogen atoms were refined anisotropically by least-squares on F^2 using the SHELXTL program.[3] The hydrogen atoms attached to carbon were placed in idealized positions and refined using a riding model to the atom to which they were attached. The molecular graphics were produced with Diamond 3.2.[4] CCDC 1449923-1449924 contain the supplementary crystallographic data for this paper. These data can be obtained free of charge via www.ccdc.cam.ac.uk/data_request/cif. Crystal data for both compounds are given in Table 1 and selected bond lengths and angles are shown in Table S1.

(1) Blessing, R. H. Acta Crystallogr., Sect. A 1995, 51, 33.

(2) Sheldrick, G. M. SADABS 2.05; University Göttingen: Gottingen, Germany, 1997.

(3) SHELXTL 6.10; Bruker Analytical Instrumentation: Madison, WI, 2000.

(4) Pennington, W. T. J. Appl. Crystallogr., 1999, 32, 1

2. Table S1. Bond valence sum calculations on Co and W centers in 1 and 2.

1			
Atom	Valence	Atom	Valence
W1	6.223	W9	6.241
W2	6.226	W10	6.232
W3	6.277	W11	6.202
W4	6.363	W12	6.171
W5	6.253	W13	6.274
W6	6.277	W14	6.207
W7	6.181	W15	6.225
W8	6.352	W16	5.960
Co1	2.068		
2			
Atom	Valence	Atom	Valence
W1	6.038	W9	6.254
W2	6.185	W10	6.354
W3	6.135	W11	6.403
W4	6.312	W12	6.094
W5	6.310	W13	6.391
W6	6.247	W14	6.146
W7	6.201	W15	6.175
W8	6.294	W16	6.286
Co2	2.032		

3. Figure S1. The XRD patterns of 1 and 2.

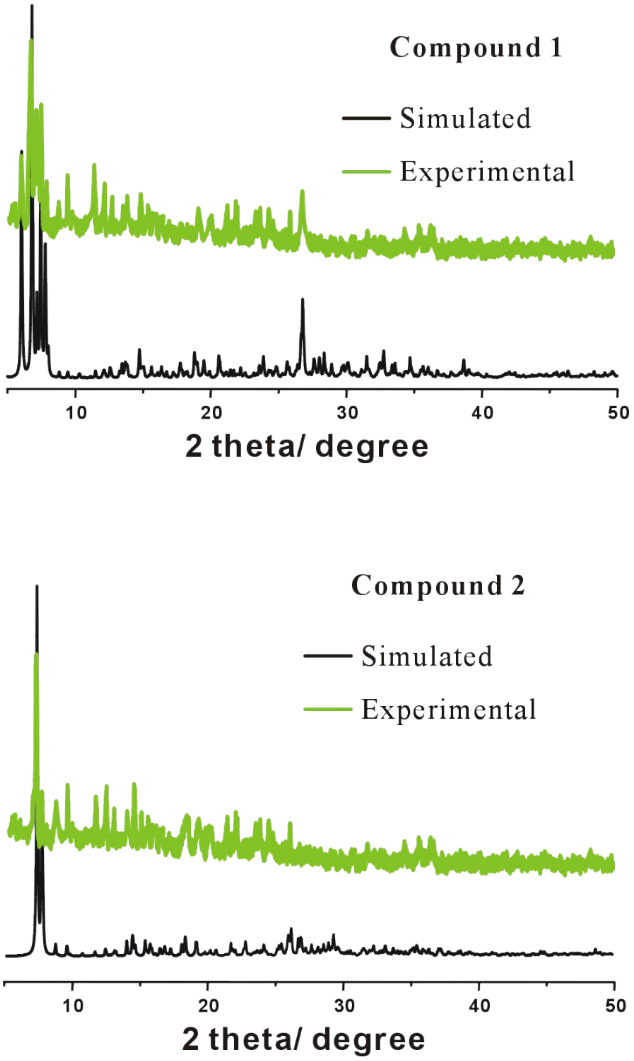

4. Figure S2. The IR for 1 and 2.

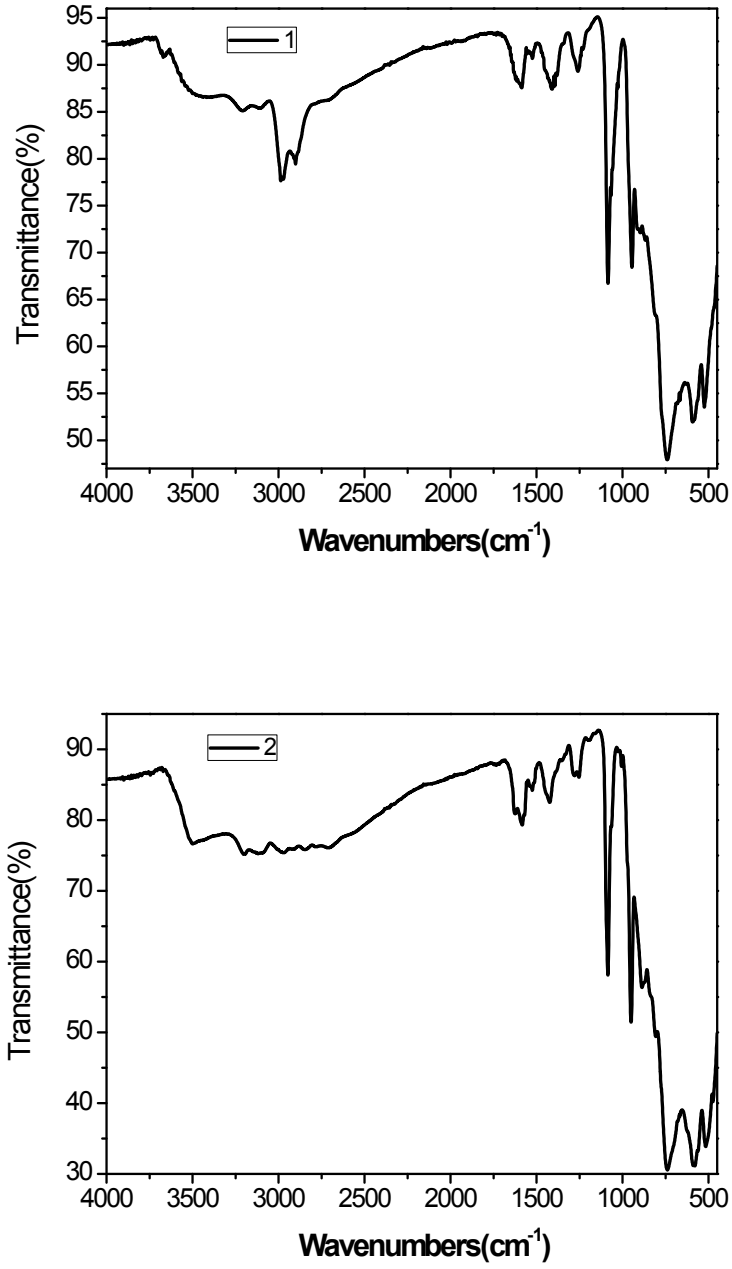

The IR spectra of 1 and 2 are shown in Figure S2, The 1 and 2 in the P-O, W-O and W-O-W stretch regions are similar suggesting that 1 resemble 2 in structure. The P-O stretching peaks appeared at 1087 and 1085 cm^{-1} for **1** and **2** respectively. And the peaks 943, 745, 585 cm^{-1} for 1 and 950, 744, 580 cm^{-1} for 2 are attributed to W-O_d, W-O_b-W and W-O_c-W vibration respectively, where O_b= double bridging oxygen; O_c= central oxygen; O_d=terminal oxygen.

5. Figure S3. The TGA curves for 1 and 2.

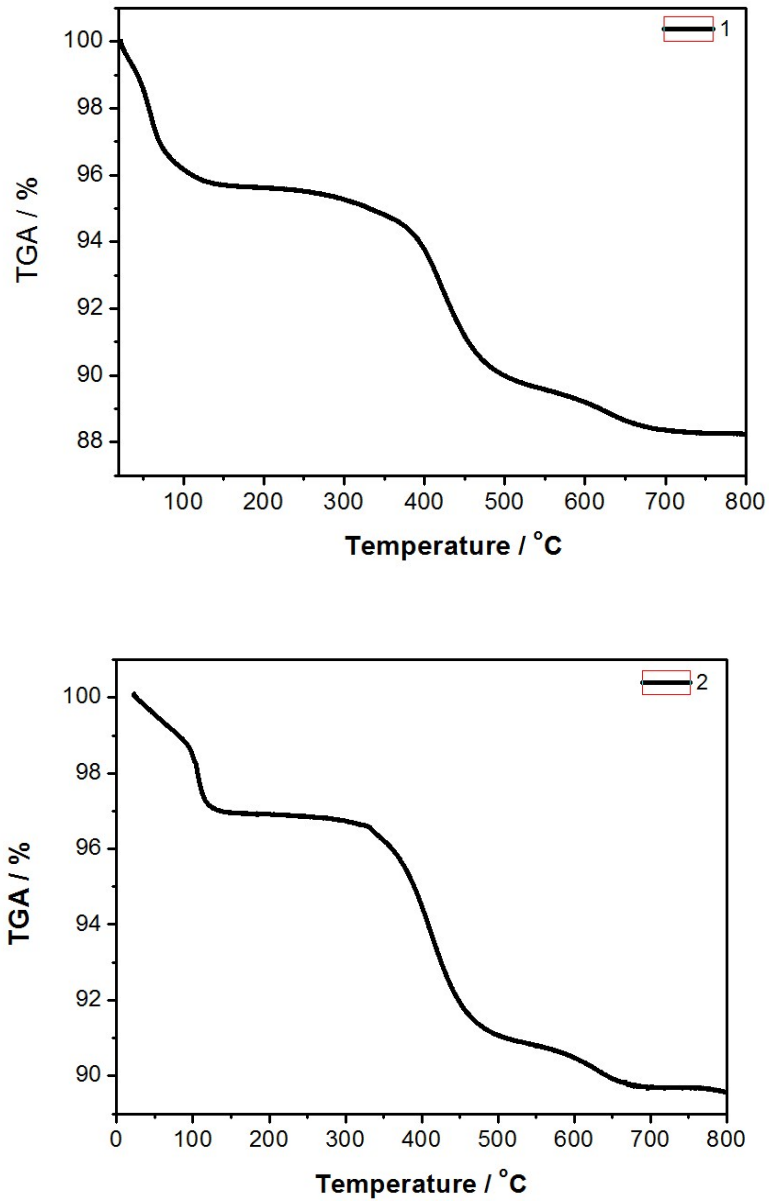

The TGA curves of 1 and 2 were investigated between 20 to 800 ^{o}C, under nitrogen atmosphere with 5 ^{o}C min^{-1} heating rate, as shown in Figure S3. There are two steps weight losing behaviour and the first weight loss of 4.1% (calc. 4.2%) from 20 to 123 ^{o}C for **1** and 2.9% (calc. 2.5%) from 20 to 127 ^{o}C for **2** which can be ascribed to the loss of water molecules, respectively. The second weight loss of 6.1% (calc. 6.1%) from 123 to 548 ^{o}C for 1 and 6.2% (calc. 6.3%) from 127 to 554 ^{o}C for 2, which can be attributed to the loss of three H_2bpz ligands.

6. Figure S4. The solid state UV-Vis for 1 and 2.

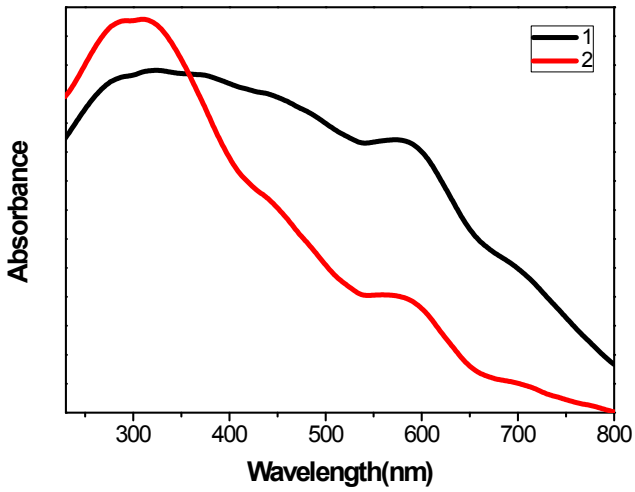

7. Figure S5. The electrocatalytic reduction ability of 1- and 2-GCE on H_2O_2

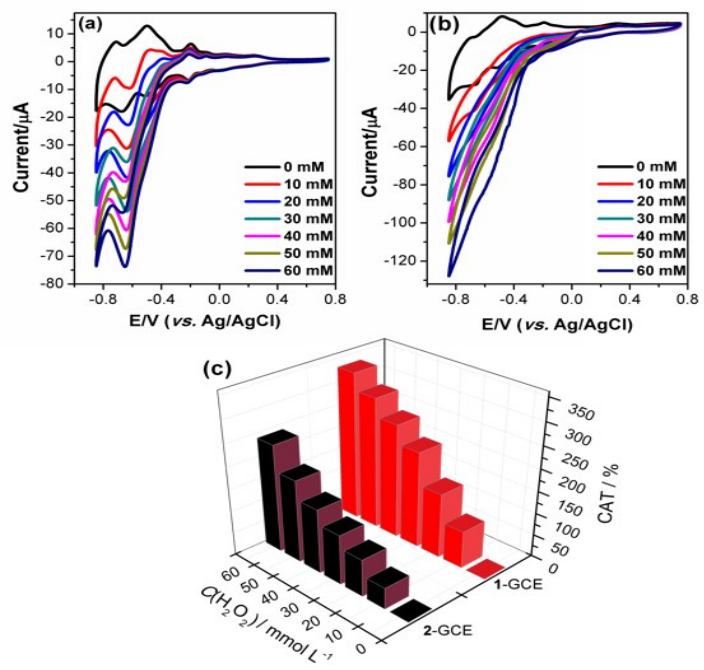

Figure S5. Cyclic voltammograms showing the catalytic activity of (a) **1**-GCE, (b) **2**-GCE in 0.5 M Na_2SO_4-H_2SO_4 aqueous solutions (pH = 2.52) with scan rate of 20 mV s^{-1}, in the presence of various concentration of. hydrogen peroxide. (c) Graph of CAT versus concentration of H_2O_2 for **1**- and **2**-GCE. (*I*p values of cathodic peak at -0.645 V for H_2O_2).

8. Figure S6. The electrocatalytic reduction ability of 1- and 2-GCE on ClO_3^-, BrO_3^-, IO_3^-

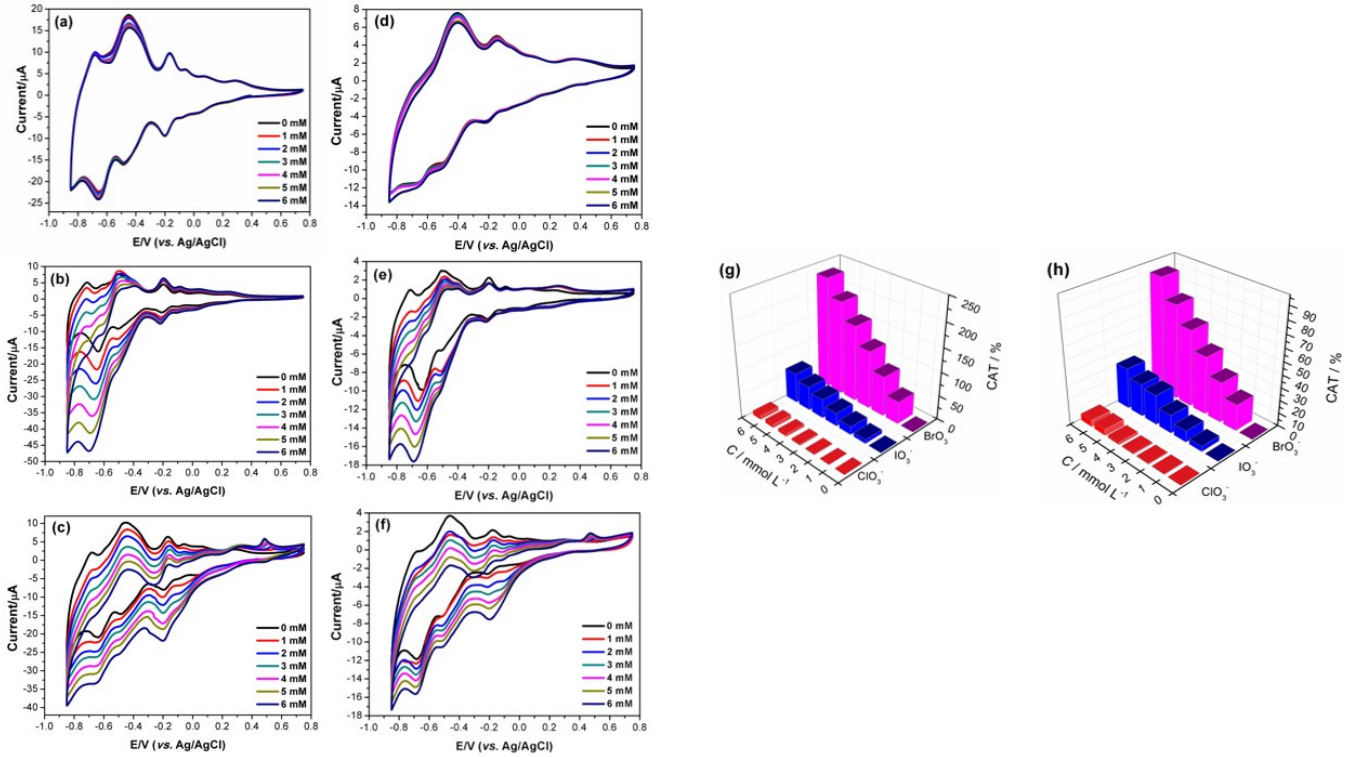

Figure S6. Cyclic voltammograms showing the catalytic activity of **1**-GCE in the presence of various concentration of (a) ClO_3^-, (b) BrO_3^-, (c) IO_3^- and that of **2**-GCE in the presence of various concentration of (d) ClO_3^-, (e) BrO_3^-, (f) IO_3^-, in 0.5 M Na_2SO_4-H_2SO_4 aqueous solutions (pH = 2.52) with scan rate of 20 mV s^{-1}. (g) Graph of CAT versus concentration of ClO_3^-, BrO_3^-, IO_3^- for **1**-GCE. (h) Graph of CAT versus concentration of ClO_3^-, BrO_3^-, IO_3^- for **2**-GCE.